applied sciences

Article

A Study on the Stress Field Around an Elliptical Wellbore with an Eccentric Casing in Deep Wells

Xiuxing Zhu [1], Bing Han [1], Yuanbo Xia [2,3], Yantao Xu [4,5], Bo Zhou [1,*] and Chengwen Wang [2,*]

1 College of Pipeline and Civil Engineering, China University of Petroleum (East China), Qingdao 266580, China; zhuxx99@upc.edu.cn (X.Z.); s23060001@s.upc.edu.cn (B.H.)
2 School of Petroleum Engineering, China University of Petroleum (East China), Qingdao 266580, China
3 CNPC Tianjin Bo-Xing Engineering Science & Technology Co., Ltd., Tianjin 300451, China
4 China Oilfield Services Limited, Tianjin 300459, China; xuyt44@126.com
5 Tianjin Key Enterprises Laboratory of Offshore Oil Reserves Exploitation, Tianjin 300459, China
* Correspondence: zhoubo@upc.edu.cn (B.Z.); wangcwupc1@126.com (C.W.)

Abstract: Casing stress distribution is one of the most relevant topics in the study of the wellbore stress field. Due to factors such as uneven geostress, the wellbore is often elliptical, and the casing may not necessarily be in the center of the wellbore. This article adopts the theory of elasticity and uses the finite element method for calculation. The main research focuses on the effects of ovality and eccentricity on the overall stress distribution of the casing and the stress distribution at the interface between the casing and cement sheath (i.e., the outer wall of the casing). The research results indicated that when the casing is centered, higher ellipticity is beneficial for improving the casing's response to non-uniform stress. However, when the casing is eccentric, higher ellipticity significantly increases the non-uniformity of the stress distribution and the risk of stress concentration in the casing. The risk of casing failure increases with increasing non-uniform stress. Additionally, a lower elastic modulus and higher Poisson ratio of the cement can improve the casing's response to stress. This research result has a certain reference value for implementing high-quality cementing construction and ensuring the normal production of oil and gas wells.

Keywords: elliptical wellbore; casing stress; non-uniform geostress

check for updates

Citation: Zhu, X.; Han, B.; Xia, Y.; Xu, Y.; Zhou, B.; Wang, C. A Study on the Stress Field Around an Elliptical Wellbore with an Eccentric Casing in Deep Wells. *Appl. Sci.* **2024**, *14*, 11888. https://doi.org/10.3390/app142411888

Academic Editor: Nikolaos Koukouzas

Received: 14 November 2024
Revised: 12 December 2024
Accepted: 17 December 2024
Published: 19 December 2024

1. Introduction

With the prolonged development time of oil fields and the increasing depth and difficulty of extraction, the technology and stress conditions of oil and water well casings have become more complex. The resulting casing damage, such as cracking, perforation, and fracture, continues to occur. These casing damage issues have become a major challenge for the development of the petroleum industry [1]. Taking the Xingbei Area of Daqing Oilfield as an example, casing damage has been a severe problem. According to reports, the number of wells with casing damage has reached 26% of the total number of producing wells [2]. This has significantly impacted the development efficiency of the oilfield. This situation increases the cost of extraction operations and has a negative impact on the well production. Indeed, this has had an adverse impact on the economic benefits of shale gas development [3].

After the completion of casing cementing, the casing, cement sheath, and formation will form a tightly bonded structure, collectively bearing the mechanical loads from various operations such as oil and gas testing, production, and fracturing. The casing is subjected to complex environmental conditions. Mechanical issues, such as casing deformation and failure, can easily occur, posing a high risk to wellbore integrity [4]. In the casing–formation–cement sheath system, the cement sheath plays a crucial role in suspending the casing and isolating the formation. It effectively delays or reduces the transfer of formation stresses to the casing, thus protecting the integrity of the casing [5]. Therefore, it is necessary to study the influence of non-uniform stress and irregular wellbore shapes on the stress distribution in the casing.

Early scholars both domestically and internationally have made idealized assumptions on the mechanical model of the casing–cement–formation system. They assumed that the wellbore shape is relatively regular and the casing is centered, while there is complete bonding between the casing, cement annulus, and formation. In relevant studies, Wang et al. [6] proposed a numerical model based on the finite element method for this situation, and Wu et al. [7] established a two-dimensional model of the composite system. Yang [8] conducted numerical simulations using the Monte Carlo method, and Tian [9] conducted research using ABAQUS finite element software, investigating the influence of the elastic modulus and Poisson ratio of the cement sheath, formation characteristics, and internal pressure of the casing on the initial failure pressure of the cement forming interface. Additionally, Chen [10] proposed an elastic solution, and Do [11] proposed a closed-form solution.

When studying wellbore problems, the assumption that the casing is located at the center of the wellbore is often not fully satisfied. In practice, the casing is prone to eccentricity due to geological factors, wellbore inclination, and uneven formation stresses [12]. Khodami [13] conducted numerical simulations of casings in eccentric states, and Erge [14] found that with an increase in pipeline eccentricity, the pressure drop decreases significantly. Gu et al. [12] discovered that eccentricity has a significant impact on the size of the interface micro-annulus. Valov [15] found that when the initial tensile (shrinkage) is combined asymmetrically with the casing, casing eccentricity does not have a significant influence on stress distribution.

Under the influence of non-uniform formation stresses, the wellbore does not always maintain a circular shape but may gradually form an elliptical wellbore. In response to this issue, Li et al. [16] studied the stress distribution characteristics of the wellbore surrounding rock in collapsible formations and proposed that under non-uniform stress conditions, the wellbore in collapsible formations will exhibit an elliptical shape. Yin [17] proposed a rapid and accurate method for evaluating casing ellipticity deformation. Wu et al. [18] successfully obtained semi-analytical solutions for stress distribution at various interfaces of the composite system using the method of complex variable functions. Zhou [19] studied the initiation characteristics of cracks in elliptical wellbores. Zhang et al. [20] obtained the analytical solutions for the stress distribution in an elliptical hole using the complex stress function method. Firme et al. [21] conducted research using the finite element method to explore the influence of wellbore ellipticity on casing stress.

Currently, there is a lack of research results regarding the stress distribution in casing with an eccentricity in an elliptical wellbore. This is mainly because solving the stress distribution in the presence of an elliptical boundary is more complex, and there is no commonly used analytical method that directly calculates the stress distribution in the casing. To address this issue, researchers commonly employed conformal transformation techniques within the framework of complex functions. This approach initially transformed the elliptical boundary into a circular boundary on an auxiliary plane, subsequently utilizing the stress function method to derive the stress distribution expression for the casing. The complexity of this methodology necessitated a rigorous verification process to ensure the congruence of the derived solutions with engineering applications. Furthermore, in scenarios involving casing eccentricity, the analytical derivation of stress distribution became notably intricate [18]. To address this gap, this study utilized the principles of elastic theory and established a finite element model of the casing cement formation system under non-uniform stress and eccentricity using finite element methods. Through calculations and analysis, the influence of eccentricity and wellbore ellipticity on the overall stress distribution of the casing and the stress distribution at the casing outer wall is investigated. Furthermore, the impact of the non-uniformity of the stress field, the elastic modulus of the cement annulus, and the Poisson ratio of the cement annulus on the extreme values of the casing outer wall stress distribution is considered.

The remaining sections of this article will be organized as follows. Section 2 defines and sets the necessary variables and parameters in detail. We will also establish a finite element model for the wellbore system under the eccentricity of the casing. In Section 3, we will utilize finite element software (Abaqus2022) to simulate the stress distribution in an eccentric elliptical wellbore under different conditions. We will consider the effects of varying ellipticity, eccentricity, and other parameters on the stress distribution. The final section will provide a summary of the entire study. We will conclude and summarize the stress distribution in eccentric elliptical wellbore casing under different conditions.

2. Finite Element Model of Eccentric Casing in an Elliptical Wellbore

2.1. Establishment of the Finite Element Model

According to the theory of elasticity, based on the geometric and force characteristics of the composite model, it can be simplified as a plane strain model. To simplify the calculation process, the following assumptions are made:

(1) The casing, cement annulus, and formation are linear elastic materials. The plastic behavior of the materials is not considered, and the influence of pore pressure on stress distribution is neglected.
(2) Assuming small displacements, the changes in casing inner and outer diameters caused by loads, as well as the changes in cement annulus thickness, are neglected.
(3) Assuming tight adhesion between all interfaces without any gaps, no debonding occurs during the deformation process.
(4) We assume that the model parts are concentric and maintain their concentric status during the deformation process.

According to the model symmetry, we selected half of the model for modeling and set the eccentricity of the wellbore. Based on the data in Table 1, we established a combined model under different casing eccentricities. Firstly, we created the casing, formation, and cement annulus as separate parts and applied the TIE contact attribute at their contact interfaces (the TIE contact property is mainly used in finite element analysis to bind two regions together so that there is no relative motion between them), as per Assumption 3. The Saint-Venant principle states that if the actual distributed load is replaced by an equivalent load, the stress and strain only change near the load application location, while the stress values are basically the same far away from the load application location. According to the principle of Saint-Venant, the stress in the surrounding formation is released after drilling, but the stress far away from the wellbore remains unaffected. To eliminate the influence of boundary effects on the results, we made the size of the formation in the combined finite element model 20 times larger than the casing size. In finite element analysis, a model size that is too small can lead to significant boundary effects, affecting the accuracy of the results. A model size 20 times larger than the wellbore diameter provides a sufficient buffer zone, ensuring that the stress distribution near the wellbore is not significantly influenced by boundary conditions. Although larger models can further reduce boundary effects, they also increase computation time and resource consumption. A 20-fold size strikes a good balance between computational efficiency and accuracy. On the bottom side of the model, we set symmetric displacement boundary conditions. On the top side of the model, we applied a maximum horizontal stress of 32 MPa, while on the left and right sides, a minimum horizontal stress of 20 MPa was applied. With the above settings, we established the physical model as shown in Figure 1.

The model utilizes a structured meshing technique and employs four-node quadrilateral elements (CPE4 elements). Grid refinement has been applied to the casing and cement annulus sections. The entire combined physical model consists of a total of 15,488 nodes and 15,240 elements, as shown in Figure 2.

Table 1 is a study on the determination of grid accuracy. By comparing the peak stress of casing with different numbers of elements, it was found that when the number of elements was 15,240, the calculation of peak stress tended to be stable, and the calculation time and resource consumption were relatively low.

The data in this study are obtained from actual data of a well in Block P13 of the Daqing Oilfield [18], including the geometric and material parameters of the casing, cement annulus, and formation, as well as the numerical values of the maximum and minimum horizontal stresses. Please refer to Table 2 for specific values.

Table 1. The relationship between grid accuracy and peak stress.

Number of Elements	Peak Stress/MPa
19,480	47.3
17,510	47.2
15,240	47.2
14,150	47.0
12,910	46.7
11,550	46.5
10,020	46.3

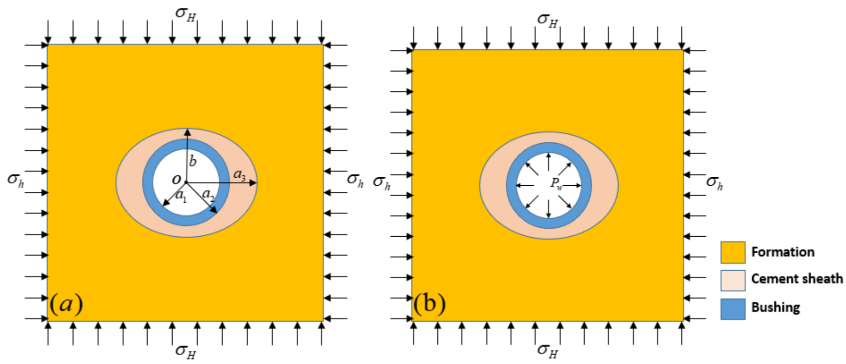

Figure 1. Model of the combination of the elliptical wellbore and eccentric casing: (**a**) physical model, (**b**) force diagram.

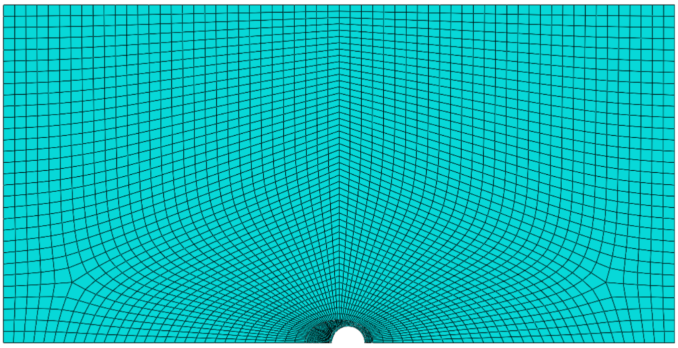

Figure 2. Finite element model of the combination body with an elliptical wellbore and eccentric casing.

Table 2. Basic parameter values, such as geometric parameters and material parameters, used in the modeling process.

Parameter	Numerical Value	Parameter	Numerical Value
a_1	78.54 mm	E_1	210 GPa
a_2	88.9 mm	E_2	20 GPa
b	107.95 mm	E_3	8 GPa
μ_1	0.32	P_w	10 MPa
μ_2	0.21	σ_H	32 MPa
μ_3	0.27	σ_h	20 MPa

Footnotes: a_1 is the inner diameter of the casing, a_2 is the outer diameter of the casing, b is the short axis of the wellbore, μ_1 is the Poisson ratio of the casing, μ_2 is the Poisson ratio of cement, μ_3 is the Poisson ratio of the formation, E_1 is the elastic modulus of the casing, E_2 is the elastic modulus of the cement sheath, E_3 is the elastic modulus of the formation, P_w is the internal pressure of the casing, σ_H is the maximum horizontal geostress, σ_h is the minimum horizontal geostress.

2.2. Variable Definition

We define ellipticity, eccentricity, and stress non-uniformity separately. In numerical simulation, we will independently vary the ellipticity and spatially uneven stress while keeping other parameters constant to investigate their respective effects on the stress distribution of the casing.

Ellipticity is a parameter that describes the degree to which the cross-sectional shape of a wellbore deviates from a circular shape. The definition of ellipticity s is as follows:

$$s = \frac{a_3}{b} \quad (1)$$

where a_3 represents the long axis of the elliptical wellbore. The value of eccentricity s is defined as 1.0, 1.1, 1.2, 1.3, 1.4, or 1.5 [18].

Stress non-uniformity is a parameter that describes the degree of uneven distribution of in situ stress around the wellbore. The definition of stress non-uniformity λ is as follows:

$$\lambda = \frac{\sigma_H}{\sigma_h} \quad (2)$$

where σ_H represents the maximum horizontal stress and σ_h represents the minimum horizontal stress. The values for stress heterogeneity are defined as 1.0, 1.1, 1.2, 1.3, 1.4, 1.5, and 1.6.

Eccentricity is a parameter that describes the degree of deviation between the wellbore axis and the major axis of the ellipse. To simplify the calculations, this study only considers the presence of eccentricity and does not take the influence of the eccentricity angle into account. Specifically, it assumes that the center of the casing and the center of the elliptical wellbore are located on the same line. Based on this assumption, we define the eccentricity as ε as follows:

$$\varepsilon = \frac{e}{b - a_1} \quad (3)$$

where e represents the eccentricity, which is the distance between the center of the casing and the center of the elliptical wellbore. b represents the major axis of the elliptical wellbore. a_1 represents the outer diameter of the casing, as shown in Figure 3.

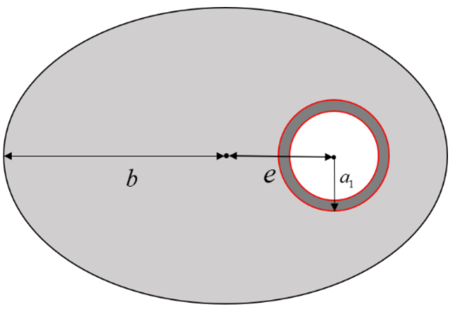

Figure 3. Overview of eccentricity.

In the subsequent numerical simulations, we will keep the elastic parameters of the casing and formation constant while varying the elastic modulus and Poisson ratio of the cement sheath. This is performed to investigate the impact of cement sheath elasticity on the distribution of casing stresses. The numerical values of the elastic parameters of the cement sheath are shown in Table 3.

Table 3. Changes in the elastic parameters of cement sheath.

Parameter	Numerical Value							
E_2/GPa	10	15	20	25	30	35	40	-
μ_2	0.12	0.15	0.18	0.21	0.24	0.27	0.3	0.33

Footnotes: E_2 is the elastic modulus of the cement sheath, μ_2 is the Poisson ratio of the cement sheath.

3. Result Analysis and Discussion

3.1. Stress Distribution of Casing Under Different Eccentricities

3.1.1. Radial Stress Distribution

In Figure 4, a contour plot of the radial stresses in the casing is shown for different eccentricities when the model reaches equilibrium. Observing the cloud map can lead to the conclusion that an increase in eccentricity leads to an uneven geometric shape of the cement sheath, which in turn leads to a complex stress distribution in the casing. The low-stress area moves towards the thinner position of the cement sheath and gradually increases its area, and the high-stress zones experience stress concentration at higher levels of eccentricity.

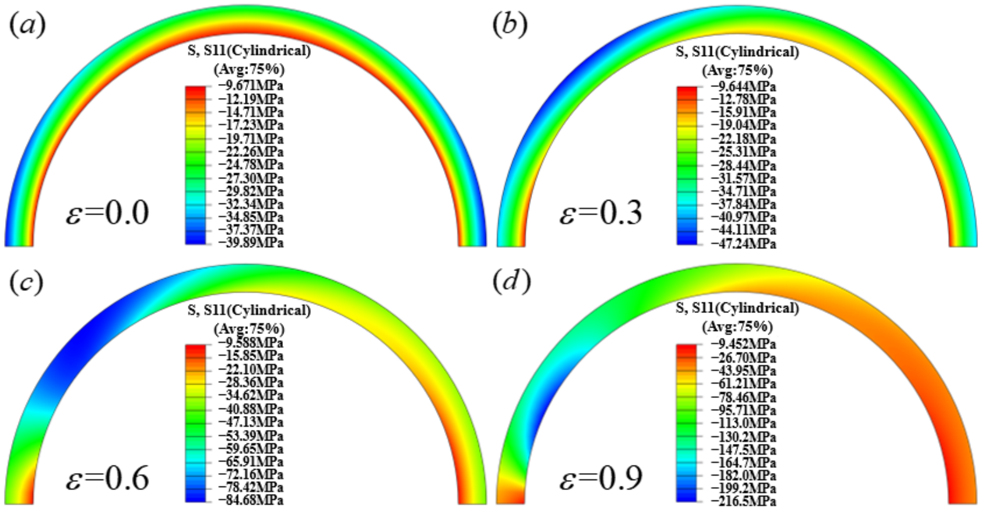

Figure 4. Radial stress distribution diagrams for different casing eccentricity values. Radial stress diagram for eccentricity: (**a**) $\varepsilon = 0.0$, (**b**) $\varepsilon = 0.3$, (**c**) $\varepsilon = 0.6$, and (**d**) $\varepsilon = 0.9$.

The specific changes in cementing are as follows: when eccentricity is 0.0, the radial stress distribution is symmetrical, with a clear transition in stress values. The low-stress zone is distributed from 0° to 180° on the inner wall of the casing. The high-stress zone is distributed between 0° to 45° and 135° to 180° on the outer wall of the casing.

When eccentricity is 0.3, the stress distribution becomes non-uniform, and the area of the low-stress zone decreases. The low-stress zone is now between 0° to 110° and 150° to 180° on the inner wall of the casing. The high-stress zone increases and is concentrated between 100° and 170° on the outer wall of the casing, particularly where the cement sheath is thicker.

When eccentricity is 0.6, the area of the low-stress region increases and is concentrated between 0° to 50° and 170° to 180° on the inner wall of the casing. The high-stress zone expands from the outer wall to the inner wall and is concentrated between 120° and 160°.

When eccentricity is 0.9, the area of the low-stress region expands and occupies most of the casing from 0° to 90°. The high-stress zone shrinks, leading to a stress concentration between 140° and 160° on the inner wall of the casing, expanding outward in a fan shape.

Figure 5 is a scatter plot obtained by extracting the radial stresses on the outer surface of the casing for each eccentricity. The overall distribution of the curves has the following characteristics:

(1) Increasing eccentricity leads to a non-uniform distribution of radial stresses on the outer surface of the casing. Table 4 provides numerical values for the maximum and minimum radial stress values on the outer surface of the casing and the stress non-uniformity coefficient for each eccentricity. Eccentricity has a significant impact on the uniformity of radial stress distribution. At high eccentricities, the non-uniformity of radial stress is higher, and stress concentration is more likely to occur.

(2) The location of the maximum radial stress varies with the change in eccentricity as follows: the location of the maximum stress is generally located where the cement ring is relatively thicker. As the eccentricity increases, the probability of stress concentration occurring also increases.

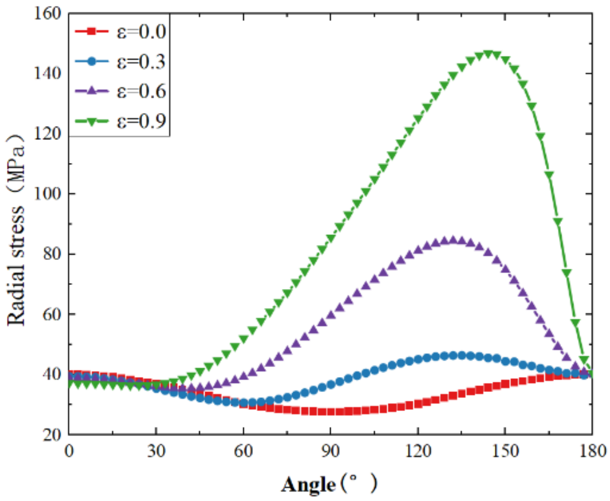

Figure 5. Radial stress distribution on the outer wall of the casing under different eccentricity ratios.

Table 4. Maximum radial stress and stress non-uniformity coefficient under different eccentricity ratios.

	ε=0.0	**ε=0.3**	**ε=0.6**	**ε=0.9**
$\sigma_{Max.r}$/MPa	40.17	46.46	84.54	146.93
$\sigma_{Min.r}$/MPa	27.75	30.76	35.48	36.51
K	1.44	1.51	2.38	4.024

Footnotes: $\sigma_{Max.r}$ is the maximum radial stress value, $\sigma_{Min.r}$ is the minimum radial stress value, and K is the stress non-uniformity coefficient.

3.1.2. Circumferential Stress Distribution

Figure 6 displays the contour plot of circumferential stress distribution in the casing at different eccentricities. By observing the plots, we can conclude that as the eccentricity increases, the non-uniformity of circumferential stress distribution and the occurrence of stress concentration become more pronounced. The increase in eccentricity leads to an increase in the non-uniformity of circumferential stress distribution in the casing, accompanied by stress concentration. The area of the low-stress region continuously increases and shifts towards the position of the thinner cement ring, while the area of the high-stress region decreases.

The specific changes in cementing are as follows. When eccentricity is 0.0, the low-stress area, 80° to 100°, is on the inner wall of the casing (thinner cement sheath), mostly near the inner wall. The high-stress zone, 0° to 20° and 160° to 180°, diverges from the inner wall to the outer wall. Both zones are symmetrical about the T-Z plane.

When eccentricity is 0.3, the circumferential stress distribution is similar to that at an eccentricity of 0.0. The low-stress zone is no longer symmetrical, with an increased area.

When eccentricity is 0.6, the low-stress zone expands and shifts towards the thicker position of the cement sheath, radiating from the inner wall to the outer wall. The high-stress zone decreases; the area on the thick cement ring side decreases the most, resulting in stress concentration.

When eccentricity is 0.9, the low-stress zone expands to half of the casing area. The high-stress zone on the thick cement ring side further decreases, indicating a significant stress concentration state.

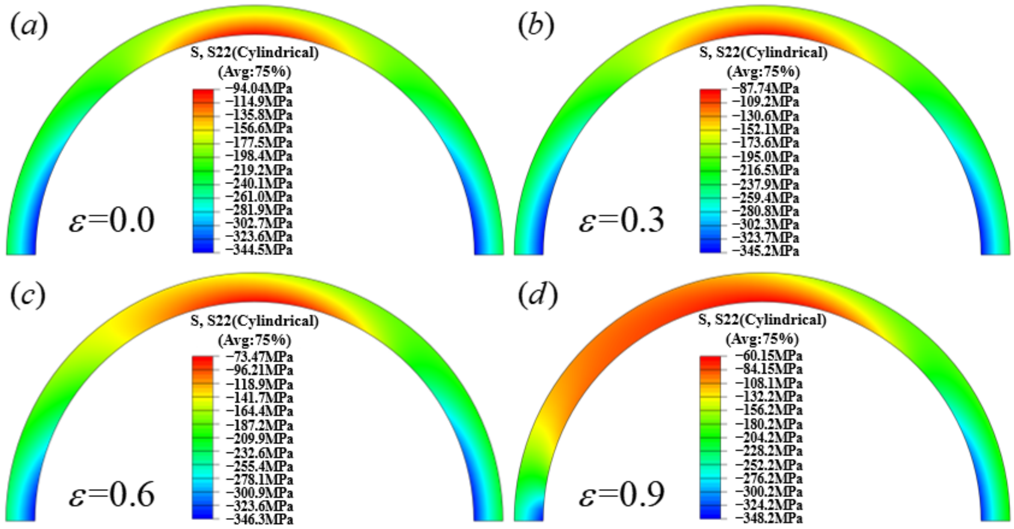

Figure 6. Circumferential stress distribution contour plot of casing at eccentricity: (**a**) $\varepsilon = 0.0$, (**b**) $\varepsilon = 0.3$, (**c**) $\varepsilon = 0.6$, and (**d**) $\varepsilon = 0.9$.

Figure 7 is a dotted line plot depicting the circumferential stress on the outer wall of the casing at different eccentricities. In the graph, the curves exhibit the following characteristics:

(1) The increase in eccentricity leads to an increase in the non-uniformity of stress distribution and the probability of stress concentration. Comparing Tables 4 and 5, we found that compared to the non-uniformity coefficient of radial stress, the non-uniformity coefficient of circumferential stress is lower. Unlike radial stress, the reason for the non-uniformity of circumferential stress is that the minimum value of circumferential stress is constantly decreasing.

(2) The increase in eccentricity reduces the value of circumferential stress on the outer wall of the casing. The maximum stress values under each eccentricity are almost the same, and the orientation of the maximum stress values under each eccentricity is 180 °, which is the thickest position of the cement sheath. The minimum stress values under different eccentricities vary greatly, and the orientation of the minimum stress values under each eccentricity is close to the side of the thick cement sheath.

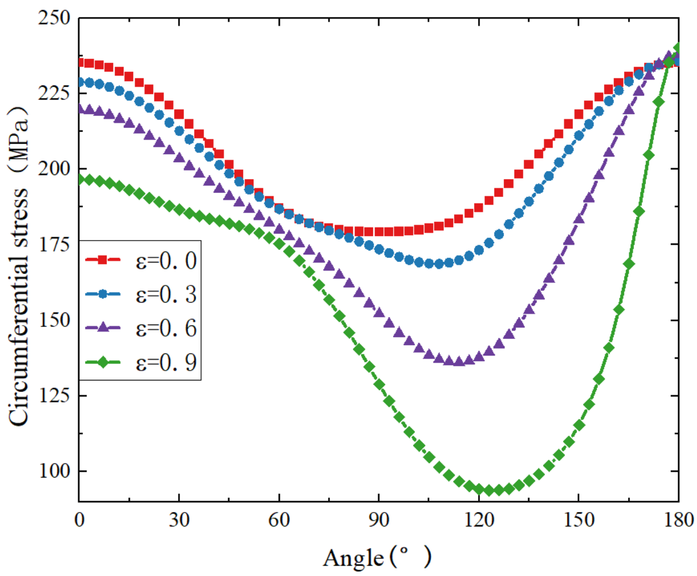

Figure 7. Circumferential stress distribution on the outer wall of the casing under different eccentricity ratios.

Table 5. Maximum circumferential stress and stress non-uniformity coefficient under different eccentricities.

	ε=0.0	ε=0.3	ε=0.6	ε=0.9
$\sigma_{Max.c}$/MPa	235.31	235.95	236.14	235.37
$\sigma_{Min.c}$/MPa	179.26	168.69	136.09	93.73
K	1.31	1.4	1.75	2.56

Footnotes: $\sigma_{Max.c}$ is the maximum circumferential stress value, $\sigma_{Min.c}$ is the minimum circumferential stress value, and K is the stress non-uniformity coefficient.

3.1.3. Shear Stress Distribution on the Outer Wall of the Casing

Figure 8 shows the distribution cloud map of casing shear stress under different eccentricities. By observing the graph, we can conclude that an increase in eccentricity leads to an uneven distribution of shear stress in the casing. As the eccentricity increases, a concentration of high-stress areas appears on one side of the thick cement sheath, and the area of the high-stress area gradually decreases, ultimately positioning on the inner wall of the casing.

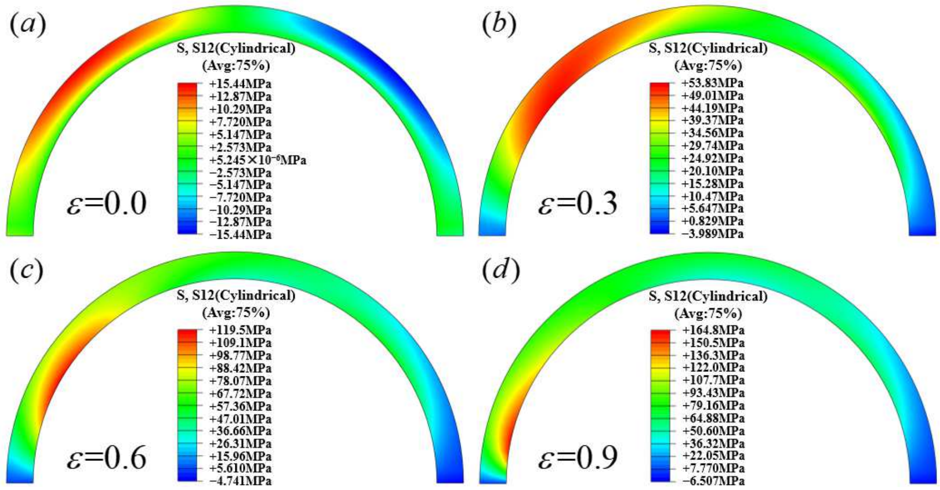

Figure 8. The distribution of casing shear stress under different eccentricity ratios. Shear stress cloud map at eccentricities: (**a**) $\varepsilon = 0.0$, (**b**) $\varepsilon = 0.3$, (**c**) $\varepsilon = 0.6$, and (**d**) $\varepsilon = 0.9$.

The specific changes in cementing are as follows. When eccentricity is 0.0, the shear stress distribution is symmetrical about the T-Z plane. The high-stress zone, 20° to 80° and 100° to 160°, is on the outer wall of the casing.

When eccentricity is 0.3, the high-stress zone moves towards the thick cement ring side. The distribution area expands from the outer wall to the inner wall of the casing.

When eccentricity is 0.6, the area of the high-stress zone decreases. The distribution zone concentrates towards the thick cement sheath and the inner wall of the casing.

When eccentricity is 0.9, the area of the high-stress zone further decreases. The high-stress zone is located on the inner wall of the casing.

Figure 9 displays a line graph of casing outer wall shear stress at different eccentricities, with the data representing absolute values of the stresses at corresponding positions on the casing. From the graph, the following conclusions can be drawn. (1) As the eccentricity increases, the non-uniformity of shear stress distribution increases, the direction of shear stress changes, and the stress values show significant increments. The specific changes are shown in Table 6. It can be observed that increasing eccentricity significantly increases the non-uniformity of shear stress distribution. (2) Based on Figure 9, it can be concluded that as the eccentricity increases, the distribution of the shear stress on the casing's outer wall becomes more non-uniform, with changes in the direction of the shear stress and significant increases in stress values. Additionally, the orientation of the maximum shear stress is typically closer to the side with a thicker cement sheath.

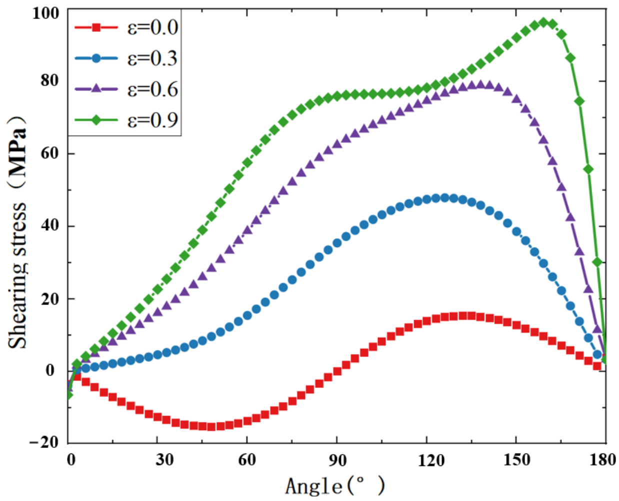

Figure 9. Distribution of shear stress on the outer wall of casing under different eccentricity ratios.

Table 6. Maximum shear stress and stress non-uniformity coefficient under different eccentricities.

	ε=0.0	ε=0.3	ε=0.6	ε=0.9
τ_{Max}/MPa	15.47	47.94	78.98	96.39
τ_{Min}/MPa	1.52	2.12	2.61	2.04
K	10.21	22.62	30.28	47.45

Footnotes: τ_{Max} is the maximum shear stress, τ_{Min} is the minimum shear stress, and K is the stress non-uniformity coefficient.

3.1.4. Mises Equivalent Stress Variation Law

Figure 10 depicts the contour plots of equivalent stress distribution in casing at different eccentricities. It can be concluded that an increase in eccentricity leads to an uneven distribution of equivalent stress in the casing. The high-stress regions shift towards the side with a thicker cement sheath, while the low-stress regions shift towards the side with a thinner cement sheath. Additionally, both the areas of high-stress regions and low-stress regions continuously increase.

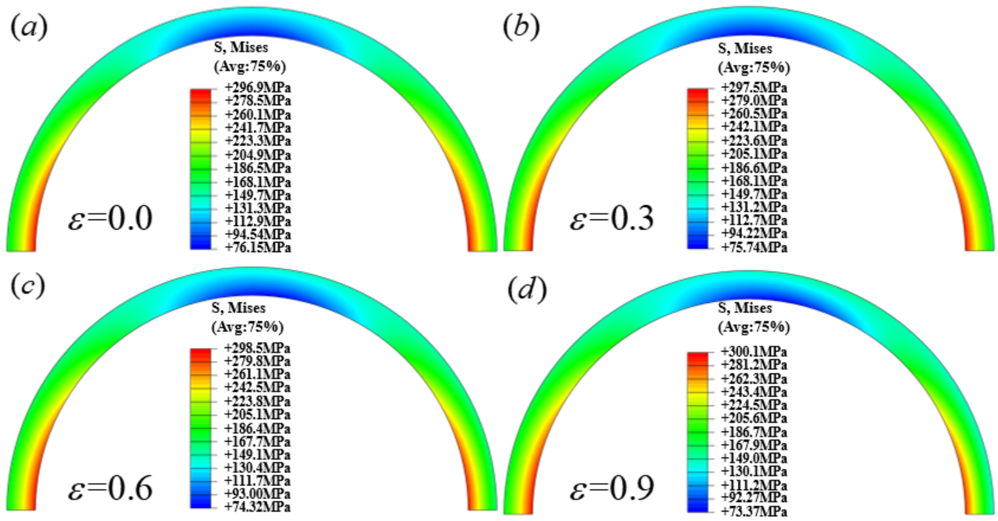

Figure 10. Equivalent stress cloud map of casing under different eccentricity ratios. Equivalent stress cloud map at eccentricities: (**a**) $\varepsilon = 0.0$, (**b**) $\varepsilon = 0.3$, (**c**) $\varepsilon = 0.6$, and (**d**) $\varepsilon = 0.9$.

Figure 11 shows the scatter plot of equivalent stress distribution on the outer surface of the casing under different eccentricities. By observing the curves, the following conclusions can be drawn: as the eccentricity increases, the stress distribution curve on the outer surface of the casing exhibits multiple extreme points. In summary, increasing eccentricity leads to fluctuations in the equivalent stress on the outer surface of the casing and the appearance of multiple extreme points. However, the maximum equivalent stress remains at the thickest part of the cement sheath. In addition, according to the data in Table 7, increasing eccentricity increases the numerical values of the maximum and minimum equivalent stresses and slightly increases the stress non-uniformity coefficient.

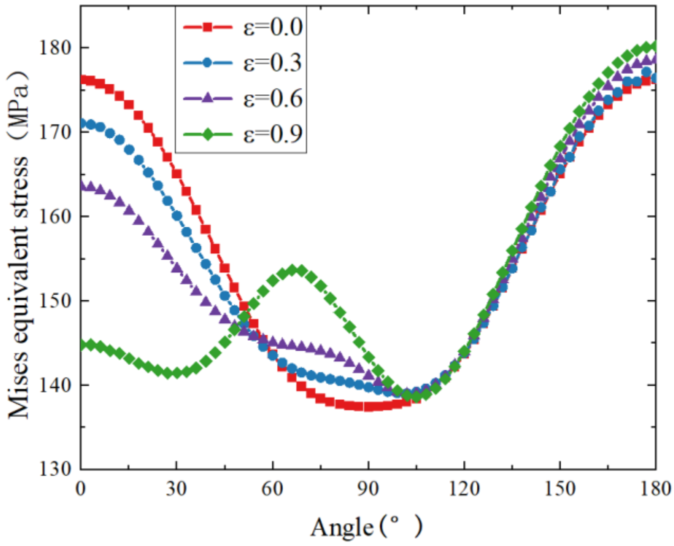

Figure 11. Equivalent stress distribution on the outer wall of casing under different eccentricities.

Table 7. Equivalent maximum stress and stress non-uniformity coefficient under different eccentricities.

	ε=0.0	ε=0.3	ε=0.6	ε=0.9
$\sigma_{Max.e}$/MPa	176.23	177.18	178.61	180.23
$\sigma_{Min.e}$/MPa	137.42	139.05	138.96	138.62
K	1.28	1.27	1.29	1.31

Footnotes: $\sigma_{Max.e}$ is the maximum equivalent stress value, $\sigma_{Min.e}$ is the minimum equivalent stress value, and K is the stress non-uniformity coefficient.

3.2. The Influence of Uneven Geostress on Casing

3.2.1. The Influence of Uneven Geostress on the Maximum Stress Component and Equivalent Stress of Casing

Figure 12 illustrates that under different eccentricity conditions, as the stress heterogeneity increases, the maximum stress on the outer wall of the casing steadily rises. It can be concluded that eccentricity has a significant influence on casing stress, and increasing stress heterogeneity leads to an increase in the maximum stress on the outer wall of the casing.

Keeping the eccentricity constant, as the stress heterogeneity increases, the changes in hoop stress and equivalent stress become more pronounced, while the changes in radial stress and shear stress remain relatively stable. Table 8 presents the increase in stress on the outer wall of the casing as the stress heterogeneity λ increases from 1.0 to 1.6. From this, we can conclude that when the eccentricity is fixed, the changes in hoop stress and equivalent stress become more pronounced as the stress heterogeneity increases. Circumferential stress and equivalent stress are more sensitive to the non-uniformity of in situ stress.

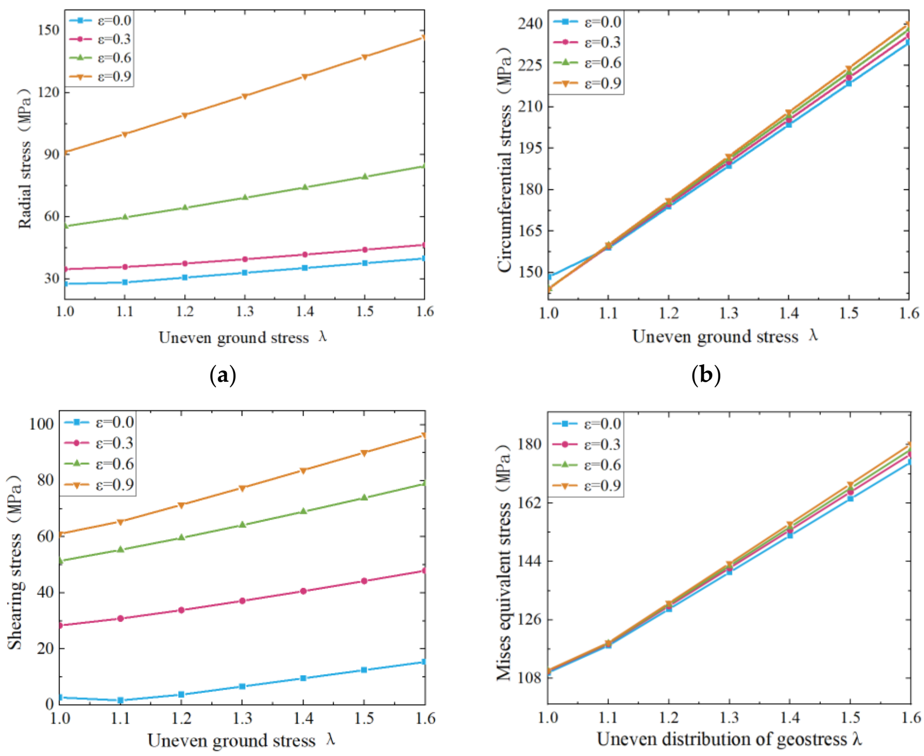

Figure 12. Maximum stress distribution on the outer wall of the casing under different geostress non-uniformities and eccentricities. (**a**) Radial stress; (**b**) circumferential stress; (**c**) shearing stress; (**d**) Mises equivalent stress.

Table 8. The increase in casing stress under different eccentricities when the unevenness of geostress increases.

	ε=0.0	**ε=0.3**	**ε=0.6**	**ε=0.9**
$\Delta\sigma_r$/MPa	12.33	11.79	29.09	55.68
$\Delta\sigma_c$/MPa	84.88	91.74	93.94	96.16
$\Delta\tau$/MPa	12.69	19.57	27.58	35.31
$\Delta\sigma_e$/MPa	64.93	66.97	68.19	69.74

Footnotes: $\Delta\sigma_r$ is the increase in radial stress, $\Delta\sigma_c$ is the increase in circumferential stress, $\Delta\tau$ is the increase in shear stress, $\Delta\sigma_e$ is the equivalent stress increase.

3.2.2. The Influence of Uneven Geostress on Casing Eccentricity

According to Table 8, when keeping the stress heterogeneity constant, we can observe that the larger the eccentricity, the overall trend of stress increase is increasing. Especially, the changes in radial stress and shear stress are the most dramatic. However, the changes in hoop stress and equivalent stress at different eccentricities are relatively small. From this, we can conclude that radial stress and shear stress are more sensitive to eccentricity, and their numerical changes are larger compared to hoop stress and equivalent stress. Therefore, when considering the influence of eccentricity on casing stress, special attention needs to be paid to the changes in radial stress and shear stress.

3.3. The Influence of the Elastic Modulus of Cement Sheath on Casing

3.3.1. The Influence of Elastic Modulus of Cement Sheath on the Maximum Stress Component and Equivalent Stress of Casing

Figure 13 shows the distribution of the maximum stress value on the outer wall of the casing under different eccentricities while keeping other conditions unchanged and changing the elastic modulus of the cement sheath.

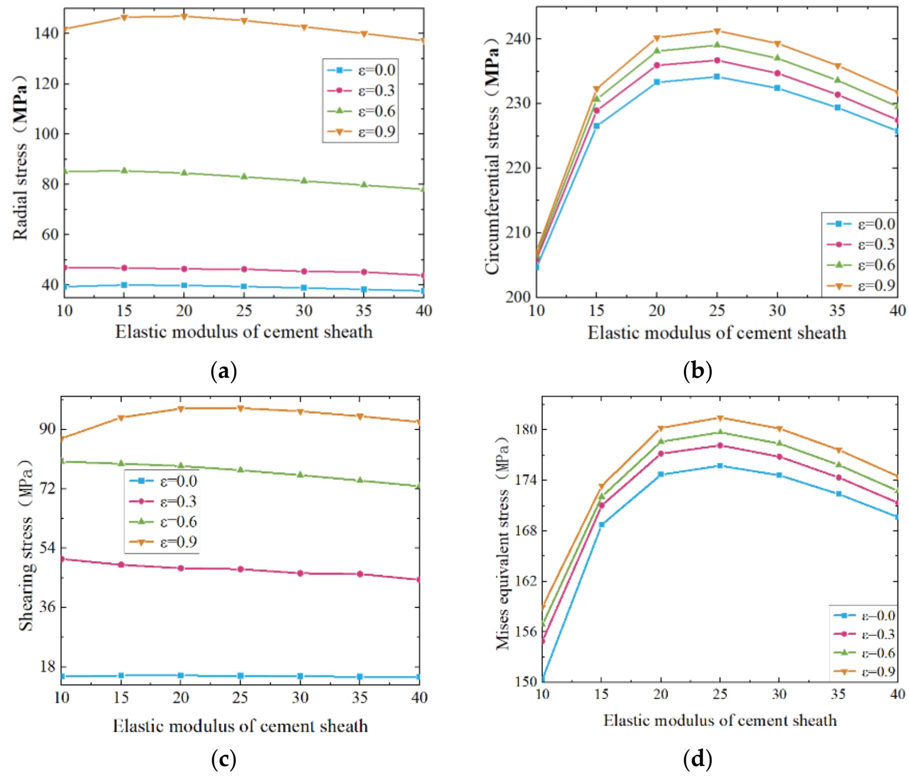

Figure 13. Maximum stress distribution on the outer wall of casing under different elastic moduli of cement sheath. (**a**) Radial stress; (**b**) circumferential stress; (**c**) shearing stress; (**d**) equivalent stress.

When eccentricity is fixed, an increase in the elastic modulus of the cement sheath has a relatively small impact on the variation of shear stress and radial stress, while it has a relatively large impact on the variation of equivalent stress and hoop stress. Specifically, let us take the changes in radial stress and equivalent stress as examples. (1) Radial stress is when eccentricity is fixed and as the elastic modulus increases, the stress value first slightly decreases and then increases. This indicates that the variation of the elastic modulus of the cement sheath has a minor impact on the radial stress. (2) Equivalent stress is when the stress variation is similar at different eccentricities, exhibiting the same pattern and peak values. When E_2 is 25 GPa, the hoop stress values reach their peak at each eccentricity. This indicates that the hoop stress value is greater under a higher elastic modulus.

3.3.2. The Influence Law of Elastic Modulus of Cement Sheath on Casing Eccentricity

Based on the specific values provided, it can be observed that with a fixed elastic modulus of the cement sheath at 25 GPa, there is a tendency for higher casing stress values as the eccentricity increases. Among them, radial stress and shear stress exhibit the most significant changes, and they are highly sensitive to eccentricity. As the eccentricity increases, the radial stress and shear stress exhibit the largest increments and the highest sensitivity to eccentricity. Additionally, the elastic modulus of the cement sheath also has a certain influence on the casing stress distribution at different eccentricities. When the eccentricity is fixed, a lower elastic modulus of the cement sheath will result in lower casing stress values, while an increase in the elastic modulus of the cement sheath leads to an increase in casing stress values.

3.4. The Influence of Poisson's Ratio of Cement Sheath on Casing

3.4.1. The Influence of Poisson's Ratio of Cement Sheath on the Maximum Stress Component and Equivalent Stress of Casing

According to the results in Figure 14, we can observe the distribution of maximum stress on the outer wall of the casing at different eccentricities when the casing, formation elastic parameters, and boundary conditions remain unchanged but the Poisson ratio of the cement sheath is varied. In the figure, as the Poisson ratio increases, the stress values on the outer wall of the casing at different eccentricities show a decreasing trend. This indicates that increasing the Poisson ratio of the cement sheath can reduce the stress values in the casing.

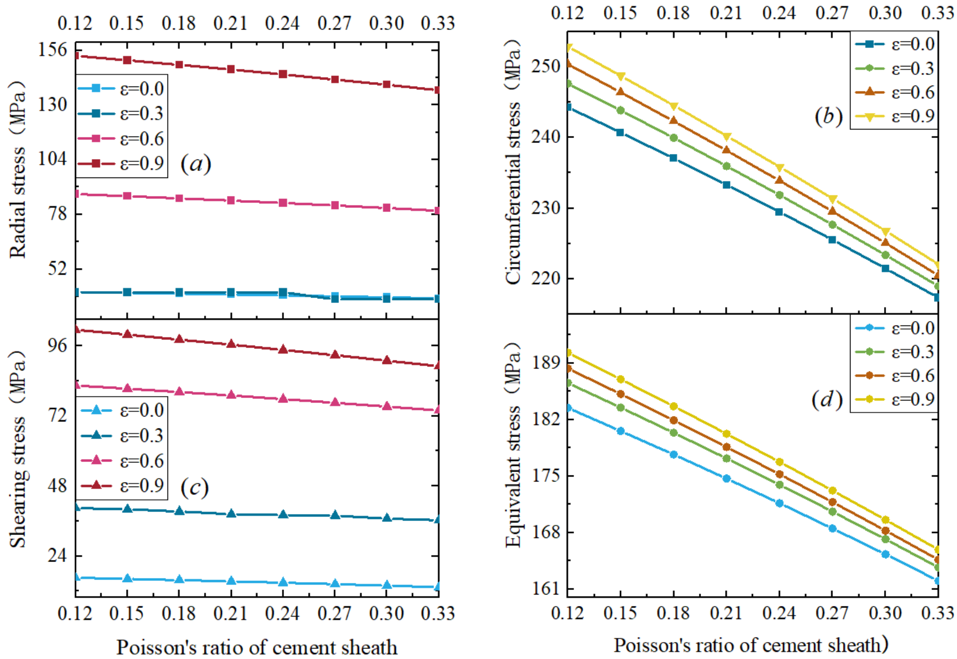

Figure 14. Maximum stress distribution on the outer wall of the casing under different Poisson's ratios of cement sheath: (**a**) maximum radial stress distribution, (**b**) maximum circumferential stress distribution, (**c**) maximum shear stress distribution, (**d**) maximum equivalent stress distribution.

3.4.2. The Influence of Poisson's Ratio of Cement Sheath on Casing Eccentricity

When the Poisson ratio of cement sheath increases from 0.12 to 0.33, the stress reduction under different eccentricity ratios is shown in Table 9. According to the results in Table 9, it can be observed that when the Poisson ratio of the cement sheath is relatively large, the stress value on the outer wall of the casing is lower, which is beneficial for improving the casing's load condition.

Table 9. Reduction in casing stress under different eccentricities when the Poisson ratio of cement sheath increases.

	ε=0.0	ε=0.3	ε=0.6	ε=0.9
$\Delta\sigma_r$/MPa	−3.01	−3.38	−7.92	−16.38
$\Delta\sigma_c$/MPa	−26.93	−28.66	−29.86	−30.75
$\Delta\tau$/MPa	−3.21	−5.26	−8.56	−12.45
$\Delta\sigma_e$/MPa	−21.38	−22.82	−23.67	−24.36

4. Conclusions

This article mainly analyzes the computational results of the elliptical wellbore casing–cement sheath–formation model under different eccentricities using numerical simulation methods. The main conclusions are as follows:

(1) Under an elliptical wellbore configuration, eccentricity significantly influences the stress distribution within the casing. As eccentricity increases, the non-uniformity of casing stress distribution becomes more pronounced. Concurrently, an increase in eccentricity results in a reduction in the high-stress zone area and an expansion of the low-stress zone.

(2) When eccentricity is held constant, an increase in the non-uniformity of geostress leads to a greater rise in equivalent stress and circumferential stress. Compared to radial stress and shear stress, equivalent and circumferential stresses exhibit higher sensitivity to variations in geostress non-uniformity. Moreover, the larger the eccentricity, the higher the stress values, even when the degree of geostress non-uniformity remains unchanged.
(3) The stress within the casing exhibits a trend of initially increasing and subsequently decreasing with changes in the elastic modulus of the cement sheath. Notably, stress values under a high elastic modulus are greater than those under a low elastic modulus. Furthermore, the presence of eccentricity amplifies the stress values within the casing.
(4) A high Poisson ratio is advantageous for improving the stress conditions of the casing, with casing stress continuously decreasing as Poisson's ratio increases.

This article only uses numerical simulation methods to analyze the stress distribution of elliptical wellbore casing under eccentric conditions, and the results may contain certain errors. In order to obtain more accurate analysis results, future research can use theories such as complex variables to derive analytical expressions for casing stress distribution and compare and analyze them with finite element results.

Author Contributions: Software, C.W.; Formal analysis, C.W.; Investigation, Y.X. (Yuanbo Xia), Y.X. (Yantao Xu) and B.Z.; Resources, X.Z., B.H., Y.X. (Yantao Xu) and C.W.; Writing—original draft, X.Z. and Y.X. (Yantao Xu); Writing—review & editing, X.Z.; Supervision, Y.X. (Yuanbo Xia) and B.Z.; Funding acquisition, Y.X. (Yuanbo Xia). All authors have read and agreed to the published version of the manuscript.

Funding: This research received no external funding.

Institutional Review Board Statement: Not applicable.

Informed Consent Statement: Not applicable.

Data Availability Statement: The raw data supporting the conclusions of this article will be made available by the authors on request.

Conflicts of Interest: Author Yuanbo Xia was employed by the company CNPC Tianjin Bo-Xing Engineering Science & Technology Co., Ltd. Author Yantao Xu was employed by the company China Oilfield Services Limited. The remaining authors declare that the re-search was conducted in the absence of any commercial or financial relationships that could be construed as a potential conflict of interest.

References

1. Yu, G.J. Theoretical Study on Casing Stress and Crush Resistance Strength Under Long-Term Stress Mechanism. Ph.D. Thesis, China University of Petroleum, Tsingtao, China, 2009.
2. Gao, A.; Shi, Y.N. Discussion on Casing Damage Warning Method in Xingbei Development Area of Daqing Oilfield. In Proceedings of the 2017 Oil and Gas Field Exploration and Development International Conference (IFEDC 2017), Chengdu, China, 21–22 September 2017; p. 12.
3. Zhao, C.J. Deformation Failure Mechanism and Experimental Study of Casing in Multi-Stage Fracturing Wells for Shale Gas. Ph.D. Thesis, China University of Petroleum, Beijing, China, 2021.
4. Guo, X.Y.; Wu, Y.Q.; Bu, Y.H.; Li, Q.; Guo, S. Elasto-plastic Analysis of Wellbore Integrity under Internal Pressure Variation. *J. China Univ. Pet. (Ed. Nat. Sci.)* **2018**, *42*, 64–69.
5. Mei, C.C. Research on Stress Distribution Inside Casing under the Coupling Conditions of Formation and Cement Ring. Master's Thesis, Southwest Petroleum University, Chengdu, China, 2014.
6. Wang, H.; Miao, M.; Zhou, T. An Analytical Approach to the Stress Distribution around a Cased Borehole in an Anisotropic Formation. *Appl. Math. Model.* **2022**, *107*, 107. [CrossRef]
7. Wu, Y.; Patel, H.; Salehi, S. Parametric Study of Mechanical Stresses within Cement Sheath in Geothermal Wells. *Geothermics* **2021**, *90*, 102000. [CrossRef]
8. Yang, S.; Zhang, R.; Wang, J.; Li, X.; Fan, H.; Yang, M. Reliability assessment of ultra-deep oil and gas wellbore casing using data statistics and numerical simulations. *J. Loss Prev. Process Ind.* **2020**, *69*, 104369. [CrossRef]

9. Tian, L.; Bu, Y.; Liu, H.; Lu, C.; Guo, S.; Xu, H.; Ren, Y. Effects of the mechanical properties of a cement sheath and formation on the sealing integrity of the cement-formation interface in shallow water flow in deep water. *Constr. Build. Mater.* **2023**, *369*, 130496. [CrossRef]
10. Chen, Z.; Zhu, W.; Di, Q. Elasticity Solution for the Casing under Linear Crustal Stress. *Eng. Fail. Anal.* **2017**, *84*, 185–195. [CrossRef]
11. Do, D.P.; Tran, N.H.; Dang, H.L.; Hoxha, D. Closed-form solution of stress state and stability analysis of wellbore in anisotropic permeable rocks. *Int. J. Rock Mech. Min. Sci.* **2019**, *113*, 11–23. [CrossRef]
12. Gu, C.; Li, X.; Feng, Y.; Deng, J.; Gray, K. Numerical investigation of cement interface debonding in deviated shale gas wells considering casing eccentricity and residual drilling fluid. *Int. J. Rock Mech. Min. Sci.* **2022**, *158*, 105197. [CrossRef]
13. Khodami, E.; Ramezanzadeh, A.; Sharifi, A. The 3D simulation of the effect of casing standoff on cement integrity by considering the direction of horizontal stresses in one of the wells of Iranian oil fields. *J. Pet. Sci. Eng.* **2021**, *206*, 108980. [CrossRef]
14. Erge, O.; Vajargah, A.K.; Ozbayoglu, O. Frictional pressure loss of drilling fluids in a fully eccentric annulus. *J. Nat. Gas Sci. Eng.* **2015**, *26*, 1119–1129. [CrossRef]
15. Valov, A.V.; Golovin, S.V.; Shcherbakov, V.V.; Kuznetsov, D.S. Thermoporoelastic model for the cement sheath failure in a cased and cemented wellbore. *J. Pet. Sci. Eng.* **2022**, *210*, 109916. [CrossRef]
16. Li, J.; Chen, M.; Zhang, G.Q.; Zhang, H. Finite Element Analysis of Casing Stress in Elliptical Wellbore of Collapse-prone Formation. *J. Univ. Pet. (Ed. Nat. Sci.)* **2004**, *28*, 45–48.
17. Yin, F.; Shi, B.; Huang, G.; Wu, X. Integrity assessment methodology of casing ovality deformation in shale gas wells. *Geoenergy Sci. Eng.* **2023**, *224*, 211643. [CrossRef]
18. Wu, S.; Fang, J.; Wang, Y.B.; He, Y.; Zhang, D. A Semi-Analytical Solution for Mechanical Characteristics of Casing-Cement Ring-Formation in Elliptical Wellbore under Non-Uniform Stress Field. *Sci. Technol. Eng.* **2022**, *22*, 997–1003.
19. Zhou, Z.L.; Guo, Y.T.; Zhang, X.; Huang, G.T. Fracture initiation from oval boreholes. *J. Pet. Sci. Eng.* **2022**, *218*, 110994. [CrossRef]
20. Zhang, K.; Chen, M. Stress distribution of cased elliptical hole with high fluid pressure: Analytical expression. *J. Pet. Sci. Eng.* **2022**, *208*, 109437. [CrossRef]
21. Firme, P.; Pereira, F.L.G.; Roehl, D.; Romanel, C. A probabilistic assessment of the casing integrity in a Pre-salt wellbore. In Proceedings of the 50th US Rock Mechanics/Geomechanics Symposium, One Petro, Houston, TX, USA, 26–29 June 2016.